Evaluation of WGA–Cre-dependent topological transgene expression in the rodent brain

Sarah Libbrecht, Chris Van den Haute, Lina Malinouskaya, Rik Gijsbers, Veerle Baekelandt

Published in Brain Structure and Function; March 2017, Volume 222, Issue 2, pp 717–733

doi: 10.1007/s00429-016-1241-x

First Online: 03 June 2016

Evaluation of WGA–Cre-dependent topological transgene expression in the rodent brain

Sarah Libbrecht [1]

Chris Van den Haute [1,3]

Lina Malinouskaya [1]

Rik Gijsbers [2,3]

Veerle Baekelandt [1,*]

Phone: +32 16 374061
Email: veerle.baekelandt@kuleuven.be

[1] Department of Neurosciences, Laboratory for Neurobiology and Gene Therapy, KU Leuven, Leuven, Belgium

[2] Department of Pharmaceutical and Pharmacological Sciences, Laboratory for Viral Vector Technology & Gene Therapy, Faculty of Medicine, KU Leuven, Leuven, Belgium

[3] Leuven Viral Vector Core, KU Leuven, Leuven, Belgium

Abstract

Novel neuromodulation techniques in the field of brain research, such as optogenetics, prompt to target specific cell populations. However, not every subpopulation can be distinguished based on brain area or activity of specific promoters, but rather on topology and connectivity. A fascinating tool to detect neuronal circuitry is based on the transsynaptic tracer, wheat germ agglutinin (WGA). When expressed in neurons, it is transported throughout the neuron, secreted, and taken up by synaptically connected neurons.

Expression of a WGA and Cre recombinase fusion protein using a viral vector technology in Cre-dependent transgenic animals allows to trace neuronal network connections and to induce topological transgene expression. In this study, we applied and evaluated this technology in specific areas throughout the whole rodent brain, including the hippocampus, striatum, substantia nigra, and the motor cortex. Adeno-associated viral vectors (rAAV) encoding the WGA–Cre fusion protein under control of a CMV promoter were stereotactically injected in Rosa26-STOP-EYFP transgenic mice. After 6 weeks, both the number of transneuronally labeled $YFP^{+}/mCherry^{-}$ cells and the transduced $YFP^{+}/mCherry^{+}$ cells were quantified in the connected regions. We were able to trace several connections using WGA–Cre transneuronal labeling; however, the labeling efficacy was region-dependent. The observed transneuronal labeling mostly occurred in the anterograde direction without the occurrence of multi-synaptic labeling. Furthermore, we were able to visualize a specific subset of newborn neurons derived from the subventricular zone based on their connectivity.

Keywords

Circuit tracing
Topological transgene expression
WGA
Transsynaptic tracer
Mouse brain

List of Abbreviations

AcbC	Accumbens nucleus, core
AcbSh	Accumbens nucleus, shell
AD	Anterodorsal thalamic nucleus
AM	Anteromedial thalamic nucleus
APT	Anterior pretectal nucleus

AV	Anteroventral thalamic nucleus
AVDM	Anteroventral thalamic nucleus, dorsomedial part
AVVL	Anteroventral thalamic nucleus, ventrolateral part
CL	Centrolateral thalamic nucleus
CPu	Caudate putamen
HDB	Nucleus of the horizontal limb of the diagonal band
IAD	Interanterodorsal thalamic nucleus
F	Nucleus of the fields of Forel
fi	Fimbria of the hippocampus
fr	Fasciculus retroflexus
LGP	Lateral globus pallidus
LM	Lateral mammillary nucleus
LDVL	Laterodorsal thalamic nucleus, ventral part
LM	Lateral mammillary nucleus
LPMR	Lateral posterior thalamic nucleus, mediorostral part
LSD	Lateral septal nucleus, dorsal part
LSI	Lateral septal nucleus, intermediate part
LSV	Lateral septal nucleus, ventral part
MD	Mediodorsal thalamic nucleus
ml	Medial lemniscus
ML	Medial mammillary nucleus, lateral part
MM	Medial mammillary nucleus, medial part
MMn	Medial mammillary nucleus, median part
MS	Medial septal nucleus
Rt	Reticular thalamic nucleus
SFi	Septofimbrial nucleus
st	Stria terminalis
Shi	Septohippocampal nucleus
sm	Stria medullaris of the thalamus
SNC	Substantia nigra, compact part
SNR	Substantia nigra, reticular part

SuML	Supramammillary nucleus, lateral part
SuMM	Supramammillary nucleus, medial part
sumx	Supramammillary decussation
VA–VL	Ventral anterior—ventrolateral thalamic nucleus
VM	Ventromedial thalamic nucleus
VPM	Ventral posteromedial thalamic nucleus
VTA	Ventral tegmental area

Electronic supplementary material

The online version of this article (doi:10.1007/s00429-016-1241-x) contains supplementary material, which is available to authorized users.

Introduction

Neuronal networks underpin behavioral and disease phenotypes. Understanding how these neuronal networks are wired and function, has emerged as a key question in the field of systems neuroscience. Visualization of these networks and subsequent manipulation are instrumental in this process. However, due to the high diversity of neurons and their ramifications, mapping the connectome requires specific labeling of small cell populations. Optogenetics allows specific and temporal manipulation of specific brain circuits using light, which has fuelled the demand for tools to label specific and distant connections.

Over the past years, the toolbox to study neuronal connectivity has expanded significantly. Earlier attempts were based on direct injections of compounds that mostly rely on axonal transport. Depending on the direction of the transport, anterograde and retrograde tracers can be discerned, such as the plant enzyme horse radish peroxidase, Fluoro-Gold and the non-toxic C fragment of the tetanus toxin (TTC) (Lanciego and Wouterlood 2011) used as retrograde tracers, and biotinylated dextran amine and its variants,

the plant lectins *Phaseolus vulgaris*—leucoagglutinin (PHA-L) and wheat germ agglutinin (WGA) as anterograde tracers (Lanciego and Wouterlood 2011). Yet, these tracers are not perfectly unidirectional but rather are transported in both directions with a preference for one direction (Lanciego and Wouterlood 2011). Modern tracing methods utilize neurotropic viruses, such as herpes simplex virus (HSV), the pseudorabies virus (PRV), and the rabies virus (RV), to efficiently cross the synapses of the first-order and higher order connected neurons (Aston-Jones and Card 2000; Boldogköi et al. 2004). However, local spread of viruses, neuroinflammation (for HSV), cytotoxicity, and strict biosafety requirements (for PRV, RV) are major limitations of these neurotropic viruses (Ginger et al. 2013).

Wheat germ agglutinin (WGA) is a plant lectin that crosses neuronal synapses following injection into the brain. WGA binds to N-acetylglucosamine and sialic acid carbohydrate residues, constituents of nerve membrane glycoproteins and glycolipids, and enters the cell through receptor-mediated endocytosis. Upon cell entry, both retrograde transport toward dendrites and anterograde transport toward axons have been documented (Fabian and Coulter 1985). Finally, following exocytosis, it can be presented to the synaptic cleft and taken up again by the next neuron (Yoshihara 2002). Indeed, studies have shown bidirectional WGA transport across synapses with preference for the anterograde direction (Braz et al. 2002; Yoshihara et al. 1999). Following WGA cloning in the late 1990s transgenic, WGA-expressing mice (Yoshihara et al. 1999) and adenoviral or adeno-associated viral (AAV) vector approaches were engineered (Kinoshita et al. 2002). Depending on the approach, choice of promoter, brain region, and time window, tracing results were different. Therefore, it appears that both the transport directionality and efficiency need to be examined for every experimental setup.

Besides unveiling the connectome, WGA transneuronal transport can also be exploited to achieve topological transgene expression for a

long period of time because of ~~to~~ its non-cytotoxic nature. In this view, Gradinaru et al. (2010) engineered a WGA and Cre recombinase fusion protein (WGA–Cre) encoded in a recombinant adeno-associated viral vector (rAAV). After stereotactic injection of rAAV2 encoding WGA–Cre unilaterally in the hippocampus (HC) together with an injection of a Cre-inducible viral vector encoding a channelrhodopsin (ChR) in the contralateral HC (cHC), topological expression of the ChR was achieved. This suggests that the combination of WGA tracer properties and optogenetic tools allows analysis and manipulation of specific brain circuits in vivo. However, a better detailed understanding of the direction and efficacy of WGA transneuronal transport is required for an optimal and widespread use of this technique.

AQ1

In this study, we aimed to measure the efficacy of rAAV-mediated WGA–Cre transneuronal tracing in different brain regions. We engineered a rAAV2/7-based vector expressing the mCherry–IRES–WGA–Cre cassette driven by a CMV promoter (referred to as rAAV2/7 WGA–Cre, see Fig. 1a) to transduce specific brain areas in ROSA26-loxP-stop-loxP-YFP (R26 YFP) reporter mice (Srinivas et al. 2001) targeting the hippocampus, the basal ganglia and the motor cortex via stereotactic injection (Fig. 1b) and the olfactory pathway via sniffing. Transduced neurons expressing both the mCherry reporter and WGA–Cre will express YFP after Cre-dependent recombination ($YFP^+/mCherry^+$). The WGA–Cre fusion protein will be transported throughout the neuron toward the synapse where it is released and taken up by the adjacent neuron via receptor-mediated endocytosis (Fig. 1a , Yoshihara 2002). Consequently, in connected neurons, Cre-dependent recombination will initiate YFP expression and mark these neurons as $YFP^+/mCherry^-$ (Fig. 1a). First, we assessed the time course of WGA–Cre-dependent tracing in the HC. Next, immunohistological analysis for YFP and mCherry was performed at 6 weeks post-injection for every brain region mentioned and the number of $YFP^+/mCherry^-$ or $YFP^+/mCherry^+$

cells was quantified.

Fig. 1

Schematic experimental overview of AAV-mediated transsynaptic tracing using WGA–Cre. **a** ROSA26-loxP-stop-loxP-YFP (R26 YFP) reporter mice were injected with rAAV2/7 CMV–mCherry–IRES–WGA–Cre or rAAV2/7 CMV–mCherry–IRES–Cre as a control, in several brain regions. Transduced neurons expressing both the reporter mCherry and the fusion protein of WGA and Cre recombinase also express YFP in a Cre-dependent manner ($YFP^+/mCherry^+$). Next, the WGA–Cre fusion protein is transported across synapses and the YFP expression is turned on in connected neurons rendering them $YFP^+/mCherry^-$. YFP and mCherry expressions were visualized by immunostaining using an Alexa488 labeled and a Cy3 labeled secondary antibody, respectively. **b** A scheme representing the different injection sites of the rAAV CMV–mCherry–IRES–WGA–Cre in mouse brain, including: the anterior olfactory nucleus (*1*), the motor cortex (*2*), the striatum (*3*), the hippocampus (*4*), and the substantia nigra (*5*)

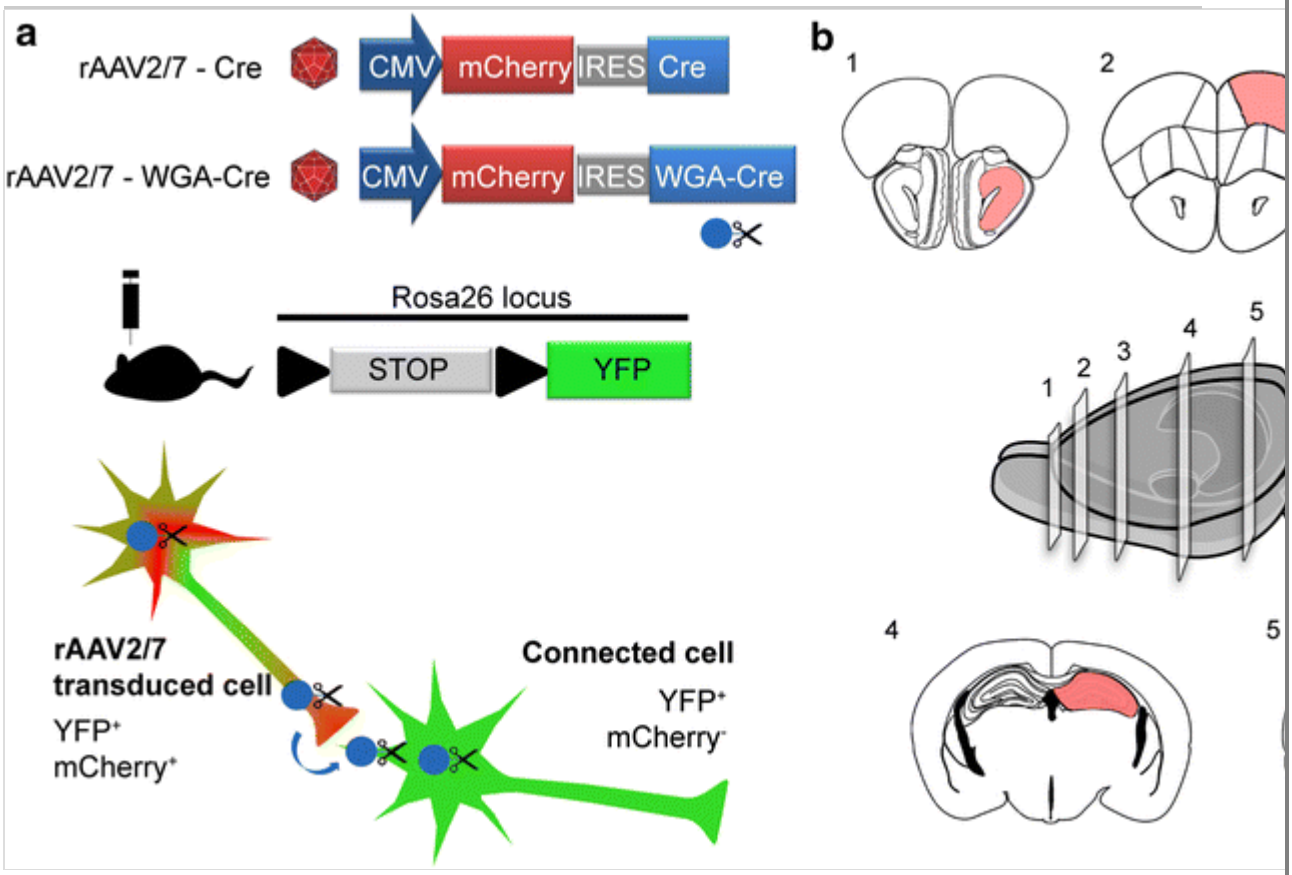

Besides studying mature neuronal networks, we wanted to employ the WGA–Cre-dependent tracing to induce gene expression in a subset of newborn neurons from the subventricular zone (SVZ) arriving in the olfactory bulb (OB). These neurons are connected by the existing bulbar network prior to integration (Deshpande et al. 2013; Kelsch et al. 2009). It has been established that in the adult brain new neurons are derived from stem cell pools residing in the SVZ and the dentate gyrus of the hippocampus (Ming and Song 2011). In the SVZ, the neural stem cells form neuroblasts that migrate through the rostral migratory stream (RMS) toward the OB, where they further differentiate into interneurons of the granule cell layer (GCL) and integrate into the network. It has been hypothesized that this integration is under tight control of the surrounding neuronal network (Kelsch et al. 2009; Whitman and Greer 2007). Indeed, rabies virus-mediated retrograde tracing showed that these progenitors are targeted by the OB network and higher olfactory areas, such as the anterior olfactory nucleus (AON) upon their arrival in the OB, prior to integration (Deshpande et al. 2013). To specifically label the newborn neurons in the OB that are connected by the AON, the latter was transduced with rAAV2/7 WGA–Cre and the connectivity analyzed at 6 weeks post-injection.

With this study, we further characterized and validated the use of WGA–Cre as an anterograde transsynaptic mapping tool in several distinct brain regions and outline the progression of labeling over time.

Materials and methods

Viral vector construction and production

Expression of the transgenes in the mouse brain was achieved using recombinant adeno-associated viral (rAAV) vectors. The mCherry–IRES–WGA–Cre expression cassette (kind gift of the Deisseroth lab) was cloned into the pAAV transfer plasmid (Van der Perren et al. 2011). Starting from this plasmid as a backbone, a pAAV

CMV–mCherry–IRES–Cre was cloned as a control. All cloning steps were sequence verified. Viral vectors were produced by the Leuven Viral vector core as described earlier (Van der Perren et al. 2011). In short, rAAV2-based vectors packaged in the AAV7-capsid were produced based on the triple transfection method with a transfer plasmid, the AAV serotype 7 plasmid (pAAV7), and the AAV helper plasmid. Viral titers were determined as DNase resistant genome copies (GC/ml) using a real-time qPCR. The genome copies obtained for rAAV2/7 CMV–mCherry–IRES–WGA–Cre and rAAV2/7 CMV–mCherry–IRES–Cre were 2.34×10^{11} GCs/ml and 1.11×10^{12} GCs/ml, respectively. Before use, the viral vector preps were titer normalized. All the experiments with rAAV vectors were performed under biosafety level 2 conditions. The respective rAAV preps are referred to as rAAV2/7 WGA–Cre and rAAV2/7 Cre.

Stereotactic injection

All animal experiments were performed in accordance with the European Communities Council Directive of November 24, 1986 (86/609/EEC) and approved by the Bioethical Committee of the KU Leuven (permit number p187/2011). Adult male and female 8–12 weeks old homozygous ROSA26-loxP-stop-loxP-YFP mice (Jax Labs, stock nr006148) were housed under a 12-h light/dark cycle with food and water ad libitum.

Anesthesia was induced by intraperitoneal injection of a mixture of ketamine (70 mg/kg, Nimatek, Eurovet) and medetomidine (1 mg/kg, Domitor, Pfizer). The mice were fixed in a stereotactic head frame (Stoelting), a midline incision of the skin was made, and a small hole drilled in the skull at the appropriate location, using bregma as reference. Appropriate vector volumes and coordinates to target the different regions were as follows:

Brain region	**Injection volume**	**Coordinates relative to Bregma (cm)**
Hippocampus	1 µl	AP 0.20; ML 0.13; DV 0.20

Brain region	Injection volume	Coordinates relative to Bregma (cm)
Striatum	2 × 100 nl	AP 0.50; ML 0.15/0.22; DV 0.30
Substantia nigra	250 nl	AP 0.31; ML 0.12; DV 0.40
Motor cortex (M1/M2)	100 nl	AP 0.25; ML 0.12; DV 0.08
Anterior olfactory nucleus	25 nl	AP 0.29; ML 0.10; DV 0.28

The viral vector was injected through borosilicate glass capillaries with a Nanoject II™ injector (Drummond) with an injection speed of 23 nl per second per increment. For the hippocampus and substantia nigra injections, increments of 41.4 nl were used, whereas for the striatum and motor cortex 23 nl and for the anterior olfactory nucleus (AON) 4.6 nl. After the injection, the needle was left in place for an additional 5 min to allow diffusion before being slowly withdrawn from the brain. Anesthesia was reversed with an intraperitoneal injection of atipamezol (0.5 mg/kg Antisedan, Pfizer). As a post-operational analgesic, buprenorfine (0.09 g/kg, Vetergesic, Patheon UK Limited) was administrated intraperitoneally.

Sniffing of the viral vector solution

Mice were anesthetized by intraperitoneal injection of a mixture of ketamine (70 mg/kg, Nimatek, Eurovet) and medetomidine (1 mg/kg, Domitor, Pfizer) . A drop of 1 µl viral vector solution was placed at the entry of one nostril and entered the nasal cavity through spontaneous respiratory breathing. This was repeated, after the drop was fully taken up, until a volume of 60 µl was applied.

Perfusion and immunohistochemistry

Mice were deeply anesthetized by intraperitoneal injection of pentobarbital (60 mg/kg, Nembutal, Ceva Sante Animale) and

perfused transcardially with saline followed by ice-cold 4 % paraformaldehyde (PFA) in phosphate buffered saline (PBS). After overnight fixation in 4 % PFA, 50-µm thick coronal brain sections were cut with a vibratome (HM 650 V, Microm). Immunohistochemistry was performed on every fifth section throughout the whole region of interest.

For single transgene staining, the free-floating sections were pretreated with 3 % hydrogen peroxide (Chem-Lab) in PBS-Triton-X100 (PBS/T) 0.1 % for 10 min and incubated overnight with rabbit anti-GFP (1:10,000, in house produced), which is also reactive against YFP, or a rabbit anti-RFP (1:5000, Rockland Immunochemicals) in PBS/T 0.1 with 10 % normal swine serum (Dako). Second, a biotinylated swine anti-rabbit (1:300, Dako) was used, followed by incubation with a streptavidin–HRP complex (1:1000, Dako). Immunoreactivity was visualized using DAB (0.4 mg/ml, Sigma-Aldrich) or Vector SG (Vector Laboratories) as a chromogen. After a dehydration series, stained sections were mounted with DPX (Sigma-Aldrich) and visualized with a light microscope (Leica Microsystems).

For fluorescent double staining, sections were washed in PBS, pre-blocked with 10 % normal horse serum in PBS/T 0.2 % and incubated overnight with rabbit anti-GFP (1:10000, produced in house) and chicken anti-RFP (1:500, Rockland Immunochemicals) in PBS/T 0.2 % with 10 % horse serum. After washing with PBS, sections were incubated for 2 h with donkey anti-rabbit Alexa488 (1:200, Molecular probes, Invitrogen) and donkey anti-chicken Cy3 (1:200, Jackson Immunoresearch) secondary antibodies in PBS/T 0.2 %. Next, the sections were washed in PBS and mounted with Mowiol. Fluorescence was detected on a laser scanning confocal microscope (FV1000, Olympus) with a laser of wavelength 488 and 543 nm.

Quantification

The number of $YFP^+/mCherry^-$ and $YFP^+/mCherry^+$ cells in the connected areas was measured with an optical fractionator method in a computerized system (Stereo Ivestigator; MicroBright-Field). A grid of $200 \times 200\ \mu m^2$ was projected over each section, and all the $YFP^+/mCherry^-$ and $YFP^+/mCherry^+$ cell bodies were counted at 20× magnification in a sampling volume of $100 \times 100 \times 13\ \mu m^3$, omitting cells in the outermost focal plane. The anatomical regions were defined using the mouse brain atlas (Paxinos and Franklin 2004). Every fifth section throughout the connected regions was analyzed resulting in absolute cell numbers in one-fifth of the brain region represented as a median.

Results

WGA–Cre-mediated transneuronal labeling in the mouse hippocampal circuit

In a first step, we set out to assess the labeling efficiency in the hippocampal circuit to corroborate transneuronal labeling after stereotactic injection in the dentate gyrus (Gradinaru et al. 2010). First, we wanted to characterize the kinetics of WGA–Cre transneuronal labeling using our AAV-based expression system. Therefore, R26 YFP mice ($n = 12$) were injected in the hippocampus (HC) of the right hemisphere with rAAV2/7 CMV–mCherry–IRES–WGA–Cre, further referred to as 'rAAV2/7—WGA–Cre', and perfused at 1 week ($n = 3$) post injection (p.i.), 3 weeks p.i ($n = 4$) and 6 weeks p.i. ($n = 5$) (Fig. 2). Evaluation of mCherry staining as a measure for transduction efficiency demonstrated a comparable targeting of the HC in the different groups (Fig. 2a). Next, immunohistochemical analysis was employed to determine Cre-induced activation of the YFP reporter in the connecting regions. For all regions investigated, a substantial increase in the number of $YFP^+/mCherry^-$ cells (full circles) was observed, whereas no significant increase was detected for the $YFP^+/mCherry^+$ labeled cells (open circles) over time (Fig. 2b–f). Transneuronal labeling

was observed as early as 1-week ~~post-injection~~p.i., albeit only to a limited extent in most of the regions. At 6-week p.i., the transneuronal labeling increased 11-fold compared to 1-week p.i. in the contralateral hippocampus (cHC) (Fig. 2b). For the Broca/MS and both the mammillary nuclei, a seven to ninefold increase was noted, whereas for the thalamus, only a fourfold increase was apparent (Fig. 2c–f). As expected, the number of $YFP^+/mCherry^+$ cells remained stable over the observed time frame (Fig. 2b–f). Hereby, we conclude that analysis at 6-week ~~post-injection~~p.i. is most suited to assess WGA–Cre-dependent transneuronal tracing.

Fig. 2

Time course of WGA–Cre transneuronal labeling in the hippocampus. **a** R26 YFP mice were injected with rAAV CMV–mCherry–IRES–WGA–Cre in the hippocampus of the right hemisphere and analyzed at 1-, 3-, and 6-week ~~post-injection~~p.i.. Immunostaining for mCherry shows a similar transduction pattern for the different time points. **b–f** Immunohistological staining against mCherry and YFP was performed, and the number of connected $YFP^+/mCherry^-$ cells and transduced $YFP^+/mCherry^+$ cells was counted in the different regions: contralateral hippocampus (cHC) (**b**), thalamus (**c**), diagonal band of Broca and medial septum (DB/MS) (**d**), supramammillary nucleus (SuMM) (**e**), and mammillary nucleus (MM) (**f**). Note the gradual increase of labeling for the connected $YFP^+/mCherry^-$ cells in all analyzed brain regions over time. The median of $n \geq 3$ mice is indicated

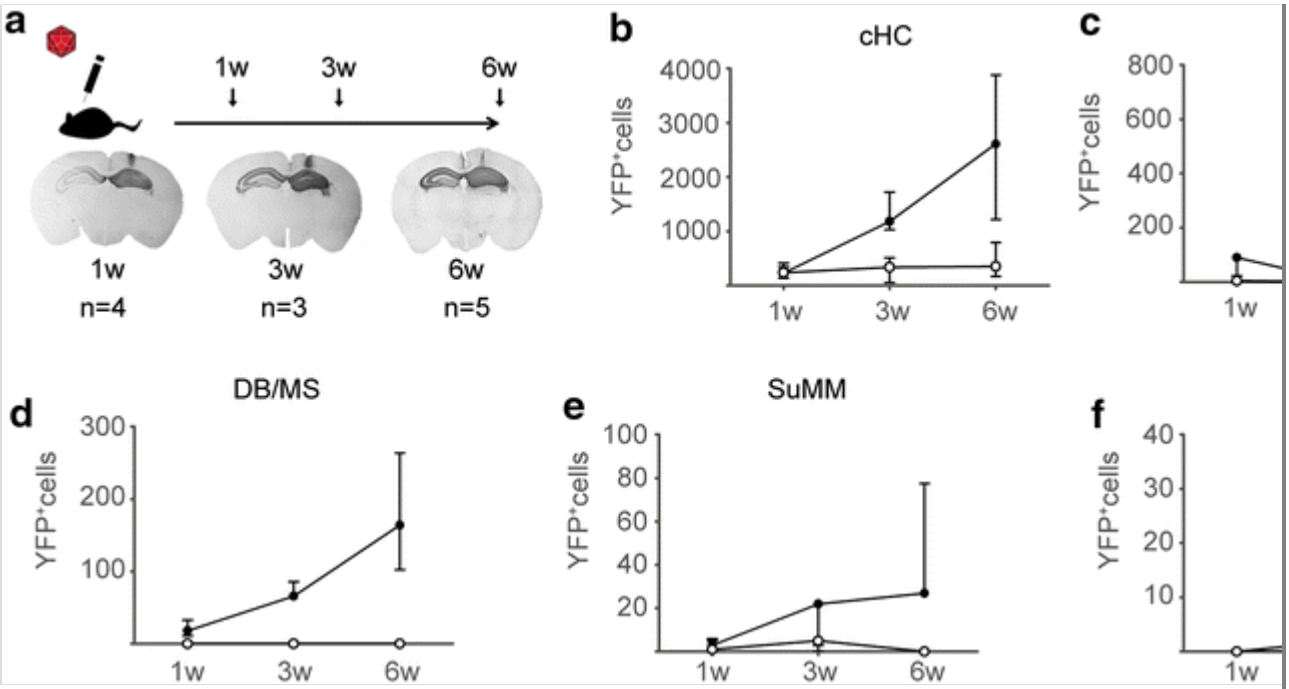

The efficiency and specificity of the transneuronal labeling was further analyzed by injection of a control group ($n = 3$) with a comparable dose (2.34×10^{11} GC/ml) of rAAV2/7 CMV–mCherry–IRES–Cre, further referred to as the 'rAAV2/7- Cre'. At 6-week p.i., immunohistochemical staining showed a similar mCherry expression pattern throughout the hippocampal region of the right hemisphere for both rAAV2/7 WGA–Cre (Fig. 3 a) and rAAV2/7 Cre (data not shown). At the contralateral side, mCherry$^+$ fiber terminals and mCherry$^+$ cell bodies were observed for both rAAV2/7 WGA–Cre and rAAV2/7 Cre (data not shown). It should be noted that the transduction of both vectors was not confined to the dentate gyrus but targeted the CA3, and to a smaller extent the CA1 region, as well.

Fig. 3

WGA–Cre-induced labeling of the interhippocampal connectome. **a** R26 YFP mice were injected with rAAV CMV–mCherry–IRES–WGA–Cre or CMV–mCherry–IRES–Cre in the hippocampus of the right hemisphere. Immunohistological staining against mCherry showed a robust transduction of the right hemisphere along the anterior-posterior axis at 6-week ~~post-injection~~p.i.. The site of injection is depicted, and the distance between two sections is

500 µm. **b** Quantification of YFP$^+$/mCherry$^+$ (*open symbols*) and YFP$^+$/mCherry$^-$ (*filled symbols*) cells through the entire cHC for both the rAAV2/7 Cre control vector (*squares*) and the rAAV2/7 WGA–Cre vector (*circles*). The median of $n \geq 3$ animals is indicated. **c** Connectivity pattern of WGA–Cre transduced neurons in the hippocampus. The injection site is marked with an *arrow*. The commissural pathway consisting of interhemisphere connectivity between both hippocampi is depicted with *full blue arrow lines* and corresponds to an anterograde direction of WGA–Cre transsynaptic labeling. The *red arrow lines* indicate the possible retrograde transsynaptic tracing originating from the injected side. Dashed lines represent labeling coming from retrogradely transduced neurons in the cHC in the anterograde and retrograde transsynaptic direction in *blue* and *red color*, respectively. *S* subiculum, and *M* molecular layer. **d** Representative superimposed tiled confocal *z*-stacks of WGA–~~cre~~Cre-dependent YFP expression in the cHC. A majority of mCherry$^-$ cells (depicted with an *arrow*) and a minority of mCherry$^+$ (depicted with an *arrowhead*) were observed. *Scale bar* 200 µm

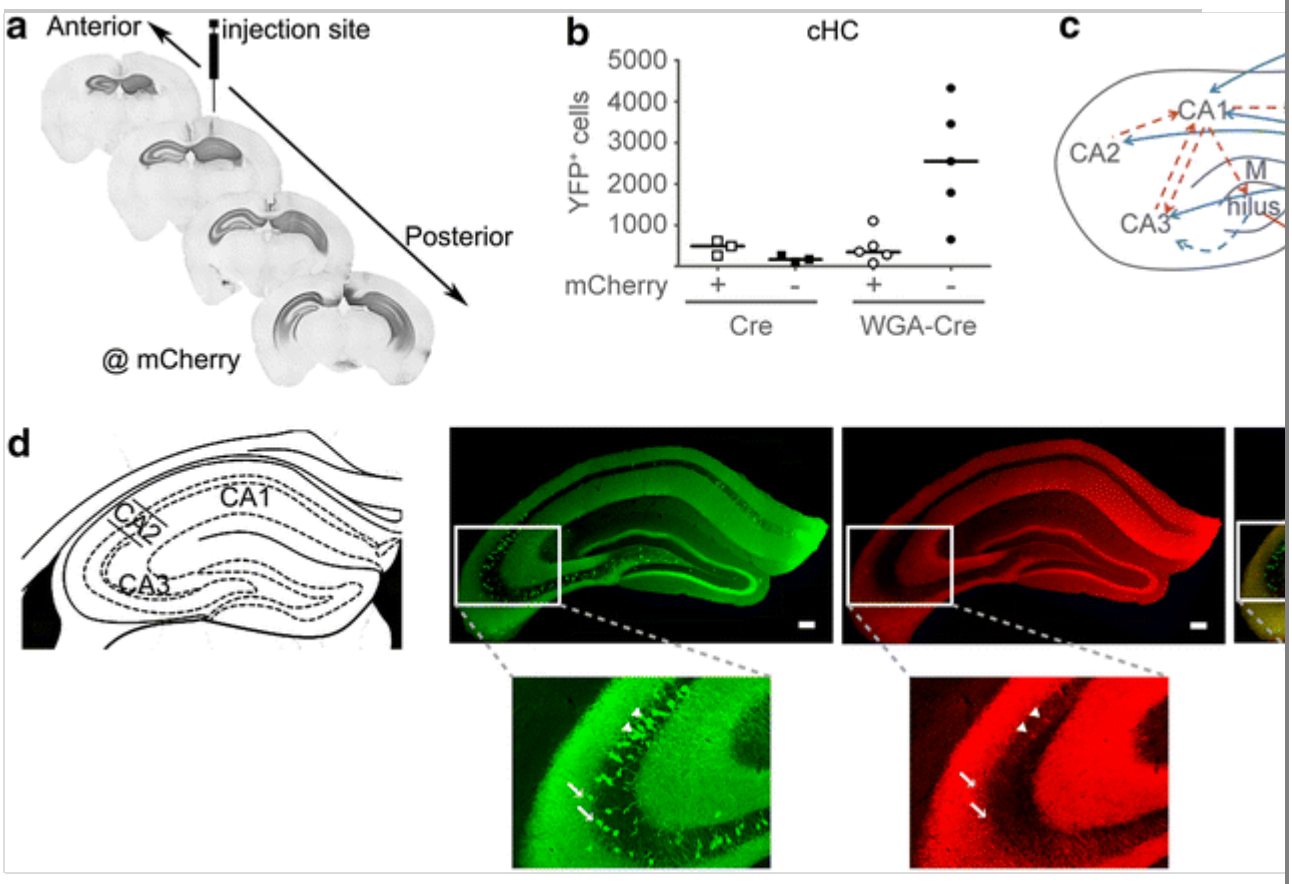

WGA–Cre induced transsynaptic labeling in the cHC was evaluated using a double fluorescent staining for YFP and mCherry (Fig. 3b, d). In rAAV2/7 WGA–Cre treated animals, $YFP^{+}/mCherry^{-}$ cells were observed in the dentate gyrus and throughout the whole cHC, with a median of 2545 (range 652–4318) cells. In the rAAV2/7 Cre treated animals, we also found $YFP^{+}/mCherry^{-}$ cells, but the number was 14-fold lower compared with the rAAV2/7 WGA–Cre condition.

Besides transneuronally labeled cells ($YFP^{+}/mCherry^{-}$), a comparable number of directly transduced ($YFP^{+}/mCherry^{+}$) cells was observed in the cHC in both groups. Due to the presence of transduced cells in the cHC, the observed transneuronal $YFP^{+}/mCherry^{-}$ expression in the cHC could result from connectivity to both the transduced cells in the injected as the non-injected cHC, as depicted by the connectome of interhippocampal connections (Fig. 3c) (Andersen et al. 2006; Witter 2010; Witter and Amaral 2004). The center of the injection is situated primarily in CA3 and the hilus as indicated by the black arrow. Consistently, these hippocampal subregions project throughout the whole cHC, suggesting an anterograde transport of the WGA–Cre fusion protein to the contralateral side. The observed $YFP^{+}/mCherry^{-}$ cells in the hilus of the cHC seem to be labeled by retrograde transport of WGA–Cre (depicted with a red arrow on the connectome). However, recurrent connections inside the hilus arising from retrogradely transduced neurons in the cHC could also explain these YFP^{+} cells (Online Resource 1). Furthermore, transduced $YFP^{+}/mCherry^{+}$ cells were found mostly in the subiculum (S) and CA1 of the cHC and could explain some of the $YFP^{+}/mCherry^{-}$ cells via the predominant pathway in which connections are made from the subiculum toward the CA1 connecting to CA2 and CA3 (indicated by red dashed lines in the cHC) Nevertheless, the low number of transduced neurons in the cHC compared with the amount in the injected area, suggests that the transsynaptic labeling observed in the cHC has its origin in the injected side. In summary, WGA–Cre

tracing in the HC occurs mostly in the anterograde direction with possible exception for the connectivity between the hilar regions.

Besides the transsynaptic labeling in the cHC, investigation of the whole rodent brain revealed transsynaptic labeling in several other regions. Regions where the number of transneuronally labeled cells was increased compared with the control included the thalamus, diagonal band of Broca and medial septum (DB/MS), and the (Supra) mammillary nuclei (Fig. 4). The $YFP^{+}/mCherry^{-}$ cells in these regions are sparser compared with the cHC. However, it should be noted that these quantifications represent an absolute number in one-fifth of the region and do not consider the volume of the area. Contradictory to the cHC, $YFP^{+}/mCherry^{+}$ cells were rarely observed in these regions for both the rAAV2/7 WGA–Cre as the rAAV2/7 Cre-injected group.

Fig. 4

WGA–Cre transgene expression in regions connected to the hippocampus. Injection of rAAV2/7 WGA–Cre in the hippocampus of the right hemisphere induced YFP expression in connected areas besides the cHC. **a**–**d** Populations of connected $YFP^{+}/mCherry^{-}$ (*filled symbols*) and transduced $YFP^{+}/mCherry^{+}$ cells (*open symbols*) were quantified for both the rAAV2/7 WGA–Cre vector (*circles*) and the rAAV2/7 Cre control vector (*squares*) in the thalamus (Thal.) (**a**), the diagonal band of Broca and medial septum (DB/MS) combined (**b**), the mammillary nucleus (MM) (**c**), and the supramammillary nucleus (SuMM) (**d**). The median of $n \geq 3$ animals is represented on the graphs. **e** Representative confocal superimposed tiled *z*-stack images of fluorescently labeled $mCherry^{+}$ and YFP^{+} cells are shown (**e**). *AD* anterodorsal thalamic nucleus; *AVDM* anteroventral thalamic nucleus, dorsomedial part; *AVVL* anteroventral thalamic nucleus, ventrolateral part; *LDVL* laterodorsal thalamic nucleus, ventral part; *HDB* nucleus of the horizontal limb of the diagonal band; *LSI* lateral septal nucleus, intermediate part; *MS* medial septal nucleus; *Shi* septohippocampal nucleus; *LM* lateral mammillary nucleus; *ML* medial mammillary

nucleus, lateral part; *MM* medial mammillary nucleus, medial part; *MMn* medial mammillary nucleus, median part; *SuML* supramammillary nucleus, lateral part; *SuMM* supramammillary nucleus, medial part; *sumx* supramammillary decussation. *Scale bars* 100 μm

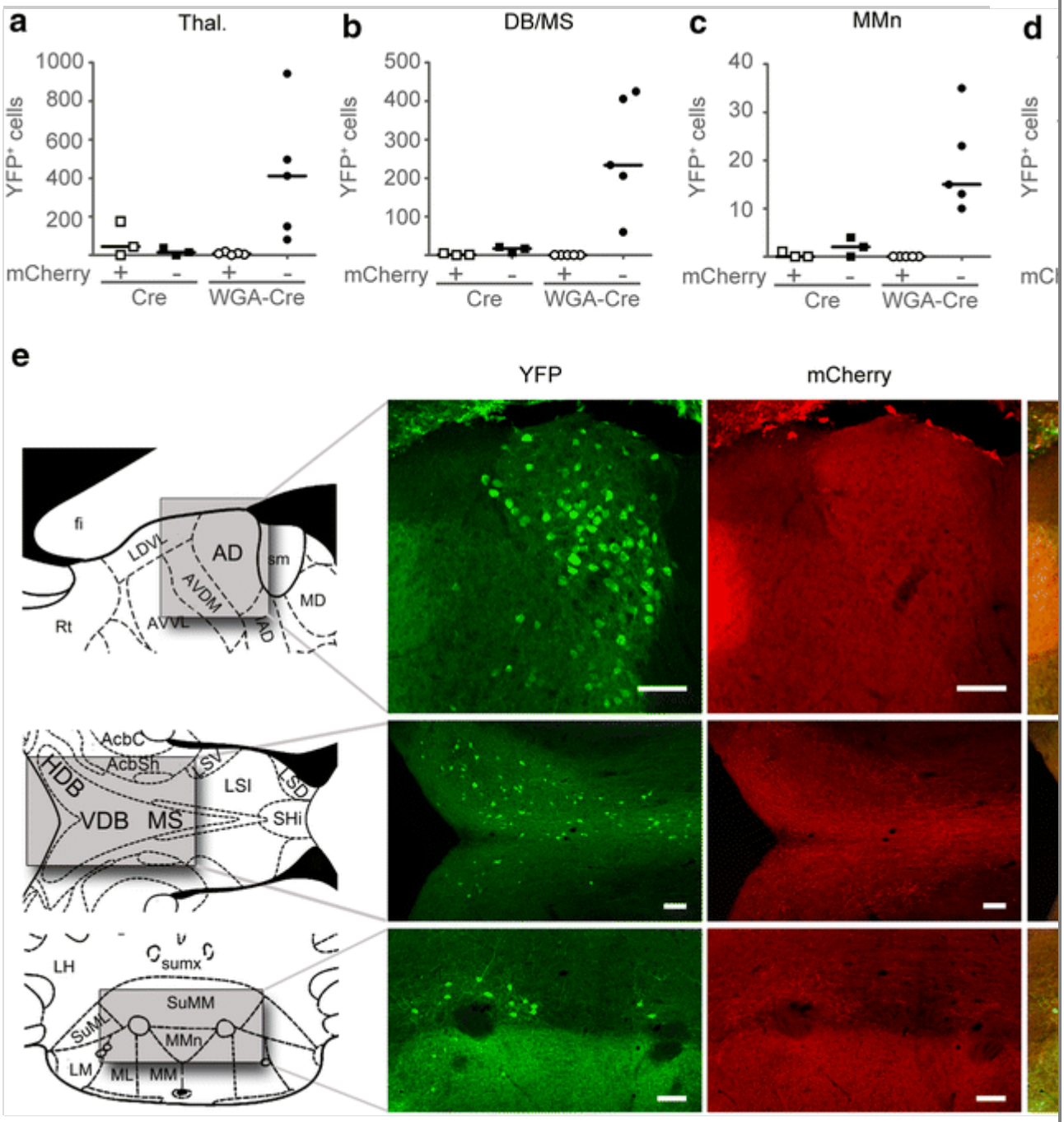

In the thalamus, predominantly in the anterodorsal nucleus (AD) ipsilateral to the injection side, a 25-fold increase in YFP^{+}/$mCherry^{-}$ cells (412; range 81–943) was found in the WGA–Cre vector group compared with the rAAV2/7 Cre treated animals (Fig. 4a, e first

panel). Also, a median of 8 YFP$^+$/mCherry$^+$ cells (range 0–18) was observed in 4 out of 5 animals of the WGA–Cre vector group. To verify the sensitivity of the reporter detection via fluorescent staining, additional single ~~staining~~stainings for mCherry ~~or~~and YFP with a biotinylated antibody was performed on consecutive sections (Online Resource 2). Although the detection of mCherry$^+$ cells was higher (a median of 54 cells was detected), the relative number of mCherry$^+$ cells in relation to the YFP$^+$ cells (a median of 263 cells) was comparable to the fluorescent staining. This suggests that the labeling is mostly due to transneuronal labeling originating in the hippocampus with a minor part of transneuronal transfer from transduced neurons in the thalamus.

In the DB/MS complex, a 13-fold increase in WGA–Cre-dependent labeled cells (237; range 60–425) was quantified after transduction with the rAAV2/7 WGA–Cre vector compared to the rAAV2/7 Cre control group (Fig. 4b, middle panel). Interestingly, no YFP$^+$/mCherry$^+$ cells were observed in animals injected with the WGA–Cre vector, whereas a few cells were detected for the rAAV2/7 Cre animals (median of 1 (range 0–5) YFP$^+$/mCherry$^+$ cells). Furthermore, these results were confirmed with a staining against mCherry with a biotinylated antibody (Online Resource 2). The transduction was centered toward the CA3 region of the HC which suggests anterograde labeling of the DB/MS complex (Gaykema et al. 1991).

In the mammillary nucleus (MM), WGA–Cre labeling led to an eightfold increase in YFP$^+$/mCherry$^-$ cells (15; range 10–35) (Fig. 4c, e bottom panel) compared with the rAAV2/7 Cre control group. In the supramammillary nucleus (SuMM), a median of 27 YFP$^+$/mCherry$^-$ cells (range 24–122) were observed, whereas none were apparent in the rAAV2/7 Cre-treated group (Fig. 4d, e bottom panel). Some YFP$^+$/mCherry$^+$ cells were observed in the SuMM, in the MM, no YFP$^+$/mCherry$^+$ cells were visible. On the mCherry$^+$ DAB staining, only a few mCherry$^+$ cells could be detected in the

MM (with a mean of 2 cells) and in the SuMM (with a mean of 9 cells) (Online Resource 2). Taken together, with a mean of 27 YFP^+ cells in the MM and a mean of 47 cells in the SuMM on the DAB staining, we can state that there is a minor increase in reporter detection, while retaining the ratio of YFP^+ cells to $mCherry^+$ cells.

Besides the above-mentioned regions in which WGA–Cre-dependent tracing has been observed and quantified, other connections were visualized by the viral vector-mediated mCherry expression (Online Resource 3). However, these connections did not result in a considerable transsynaptic labeling.

WGA–Cre transneuronal tracing in basal ganglia

In addition to the HC circuitry, we also examined whether the WGA–Cre-dependent transgene expression is suited to interrogate and study the basal ganglia connectivity and, more specifically, the connectivity between the caudate putamen (CPu) and the substantia nigra (SN). It is established that there is reciprocal connectivity between the CPu and the substantia nigra (SN) and that this connectivity might be affected in health (e.g., normal aging) and disease (e.g., Parkinson's disease) (Gerfen 2004).

First, the connectivity of the striatum to the SN was assessed. The striatum can be subdivided based on the input from the cortex or the output to different compartments of the SN (Joel and Weiner 2000; Voorn et al. 2004). According to the cortical input, there is a medial to lateral division consisting of the motor striatum followed by the associative striatum and finally the limbic striatum. The injection site was based on the morphological defined CPu (Paxinos and Franklin 2004) and the resulting transduction pattern included all subdivisions (Fig. 5a). Immunohistological quantification at 6-week p.i. showed a median of 75 $YFP^+/mCherry^-$ cells (range 49–101) in the SN (Fig. 5b, e upper panel). However, due to retrograde transduction, a median of 16 $YFP^+/mCherry^+$ cells (range 4–24) were detected as well. On the single $mCherry^+$ staining, performed

with a biotinylated antibody on the consecutive sections, a higher number of mCherry^{+} cells (mean = 41 cells) were quantified (Online Resource 4). Consequently, the transneuronal labeling in the SN may have its origin in the transduced cells in the striatum or in the SN via recurrent connectivity to the retrogradely transduced neurons. Less YFP^{+}/mCherry^{-} cells (median of 13 cells, range 7–21) were detected in the ventral tegmental area (VTA), described to reciprocally connect only with the limbic striatum, overlapping with the most medial part of the CPu. Remarkably, almost no directly transduced cells (a median of 1 cell, range 0–7) occurred in the VTA. This absence of mCherry^{+} cells was confirmed on the single mCherry staining (Online Resource 4). In short, transneuronal labeling from the striatum toward the VTA and the SN was detected; however, the directionality could not be defined. Also, a small number of cells were observed in the nucleus accumbens and the lateral hypothalamic area (Online Resource 5).

Fig. 5

Transneuronal tracing in the basal ganglia. **a** Two injections of rAAV2/7 CMV–mCherry–IRES–WGA–Cre were performed in the striatum, as indicated by the two injection tracts underneath the syringe, resulting in a transduction of the striatum along the anterior–posterior axis as shown by histological detection of mCherry expression. The injection site is depicted, and the distance between sections is 250 µm. **b** Transneuronal tracing originating from the transduced striatum occurred in the substantia nigra pars compacta (SNC) and the ventral tegmental area (VTA) at 6-week ~~post-injection~~p.i.. Both the transduced YFP^{+}/mCherry^{+} (*open circles*) and the connected YFP^{+}/mCherry^{-} (*filled circles*) cells were quantified. **c** Injection of rAAV CMV–mCherry–IRES–WGA–Cre in the SN led to a robust mCherry expression of the SN along the anterior–posterior axis. The injection site is depicted, and the distance between sections is 250 µm. **d** WGA–Cre-dependent transneuronal labeling was evident mostly in the caudate putamen (CPu), and second, in the nucleus accumbens (Acc) and the globus pallidus (GP).

Transduced YPF^{+}/mCherry^{+} (*open circles*) and connected YFP^{+}/mCherry^{-} (*filled circles*) cells were quantified. **e** Representative superimposed tiled confocal *z*-stack images of circuit tracing from the striatum to the SNC (*first panel*) and from the SN to the CPu in striatum (*second panel*) are shown. Note that in the insets with a magnified image of the SNC, both connected YFP^{+}/mCherry^{-} (*white arrow*) and transduced YFP^{+}/mCherry^{+} (*white arrowhead*) cells are present. In the CPu, mostly transsynaptic YFP^{+}/mCherry^{-} cells were found. *CPu* Caudate putamen; *SNC* substantia nigra, compact part; *SNR* substantia nigra, reticular part; *VTA* ventral tegmental area; *LGP* lateral globus pallidus. In (**b**) and (**d**), the median of $n = 4$ mice is indicated. *Scale bar* 100 μm for striatum, 200 μm for SN

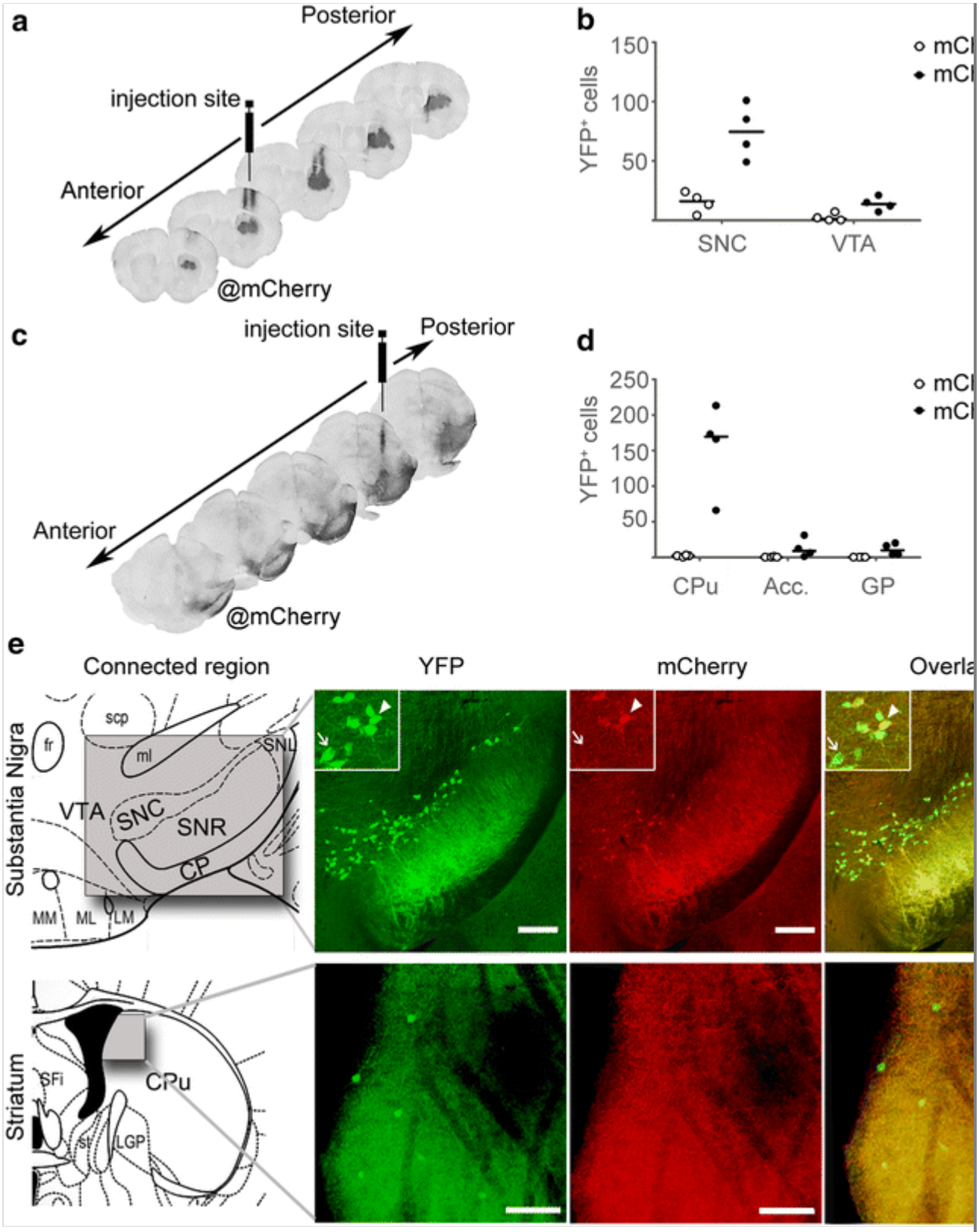

Second, the traceability of the nigral connections was assessed by injection of the WGA–Cre vector in the SN (Fig. 5c). Via immunohistological analysis, the highest labeling was detected in the CPu, containing a median of 169 $YFP^{+}/mCherry^{-}$ cells (range 66–213), and to a smaller extent in the nucleus accumbens (Acc.)

and the globus pallidus (GP) (Fig. 5d, e lower panel). Interestingly, $YFP^{+}/mCherry^{-}$ cells were detected in close proximity of the ventricles coinciding with the limbic and associative striatum (Fig. 5e, lower panel). Both in the double fluorescent staining and in the mCherry DAB staining, no $mCherry^{+}$ cells were visible in the CPu, GP, and Acc (Online Resource 6). It has been described that the associated and the limbic striatum are innervated mainly by the VTA with some contribution of the medial SN pars compacta (SNC). In reverse, the limbic striatum innervates both the SNC and the VTA, while the associated striatum innervates only the SNC (Joel and Weiner, 2000). As can be seen from the transduction pattern, both the SN and the VTA were efficiently transduced, and this could explain the labeled cells specifically in the limbic striatum. Since the limbic striatum contains more labeled cells, this could point toward a more efficient labeling in the VTA compared with the SN. The observed labeling in the GP and the Acc., although very weak, can only be explained by retrograde labeling (Deniau 1994; Gerfen 2004). This low amount of retrograde transsynaptic labeling again suggests the preference for anterograde labeling. Besides the regions listed above, $mCherry^{+}$ fiber terminals were observed in other regions as well without the occurrence of efficient YFP labeling (Online Resource 7).

In conclusion, the transneuronal labeling originating from the SN is higher compared with that stemming from the striatum. Due to the reciprocal connectivity of these regions, it was, however, impossible to conclude on the labeling directionality based on immunohistochemical data.

WGA–Cre-mediated expression in the motor cortex–thalamus pathway

Next, we injected the WGA–Cre vector in the motor cortex to assess the connectivity in the motor cortex–thalamus pathway. The transduction pattern depicts a robust lateral–medial transduction of the cell bodies in the motor cortex and more posterior the efferent

fibers toward the thalamus were apparent (Fig. 6a). Immunohistochemical analysis showed a significant number of $YFP^+/mCherry^-$ cells in several nuclei of the ipsilateral thalamus, while almost no $YFP^+/mCherry^+$ cells were present (Fig. 6b, c). These results were confirmed on single staining performed with biotinylated ~~antibiodies~~antibodies (Online Resource 8, 9). It is established that the connectivity between the motor cortex and the thalamus is stronger ipsilateral, although there is a weak cross-connectivity to the contralateral side (Carretta et al. 1996; Haber and McFarland 2001). In line, we observed almost no YFP^+ cells in the contralateral thalamus (data not shown). In the literature, it has been described that most of the connections between the motor cortex and the thalamus are reciprocal making it difficult to state the directionality of labeling. The thalamic nuclei involved in this connectivity are mostly the medial thalamic nuclei, such as the mediodorsal nucleus (MD) and the (ventral anterior) VA—ventrolateral (VL) complex (Carretta et al. 1996; Haber and McFarland 2001; Rouiller and Welker 2000). Accordingly, we observed most $YFP^+/mCherry^-$ cells in the medial nuclei, with a median of 16 cells (range 5–43) in the anteromedial nucleus (AM) and 39 cells (range 17–76) in the MD (Fig. 6b, c). In the VA–VL complex, a lower number of $YFP^+/mCherry^-$ cells with a median of 7 cells were counted. Furthermore, connections from the motor cortex to the posterior and paracentral (PC) nuclei were described in ~~rodent~~rodents and to the reticular nucleus (Rt) in cats (Carretta et al. 1996; Rouiller and Welker 2000). In these nuclei as well, a small number of $YFP^+/mCherry^-$ cells ~~were~~was found.

Fig. 6

WGA–Cre expression in the motor cortex leads to transsynaptic labeling in the thalamus. **a** 6-week ~~post-injection~~p.i. of the rAAV CMV–mCherry–IRES–WGA–Cre in the motor cortex, mCherry expression was detected via immunohistochemistry. Note the $mCherry^+$ fibers arriving in the thalamus. **b** Connected $YFP^+/mCherry^-$ and transduced $YFP^+/mCherry^+$ cells were counted

separately in several thalamic nuclei listed below. The highest number of connected YFP^+/$mCherry^-$ cells was found in the AM and MD. The median of $n = 4$ mice is indicated. *Rt* Reticular nucleus; *VA–VL* ventral anterior–ventrolateral nucleus; *Po* posterior thalamic nuclear group; *AM* anteromedial nucleus; *MD* mediodorsal nucleus; *PC* paracentral nucleus. **c** Example of a superimposed confocal *z*-stack image indicates the transneuronal labeling in the MD. *AD* anterodorsal thalamic nucleus; *AM* anteromedial thalamic nucleus; *AV* anteroventral thalamic nucleus; *CL* centrolateral thalamic nucleus; *MD* mediodorsal thalamic nucleus; *VA–VL* ventral anterior—ventrolateral thalamic nucleus; *VM* ventromedial thalamic nucleus; *Scale bars* 100 µm

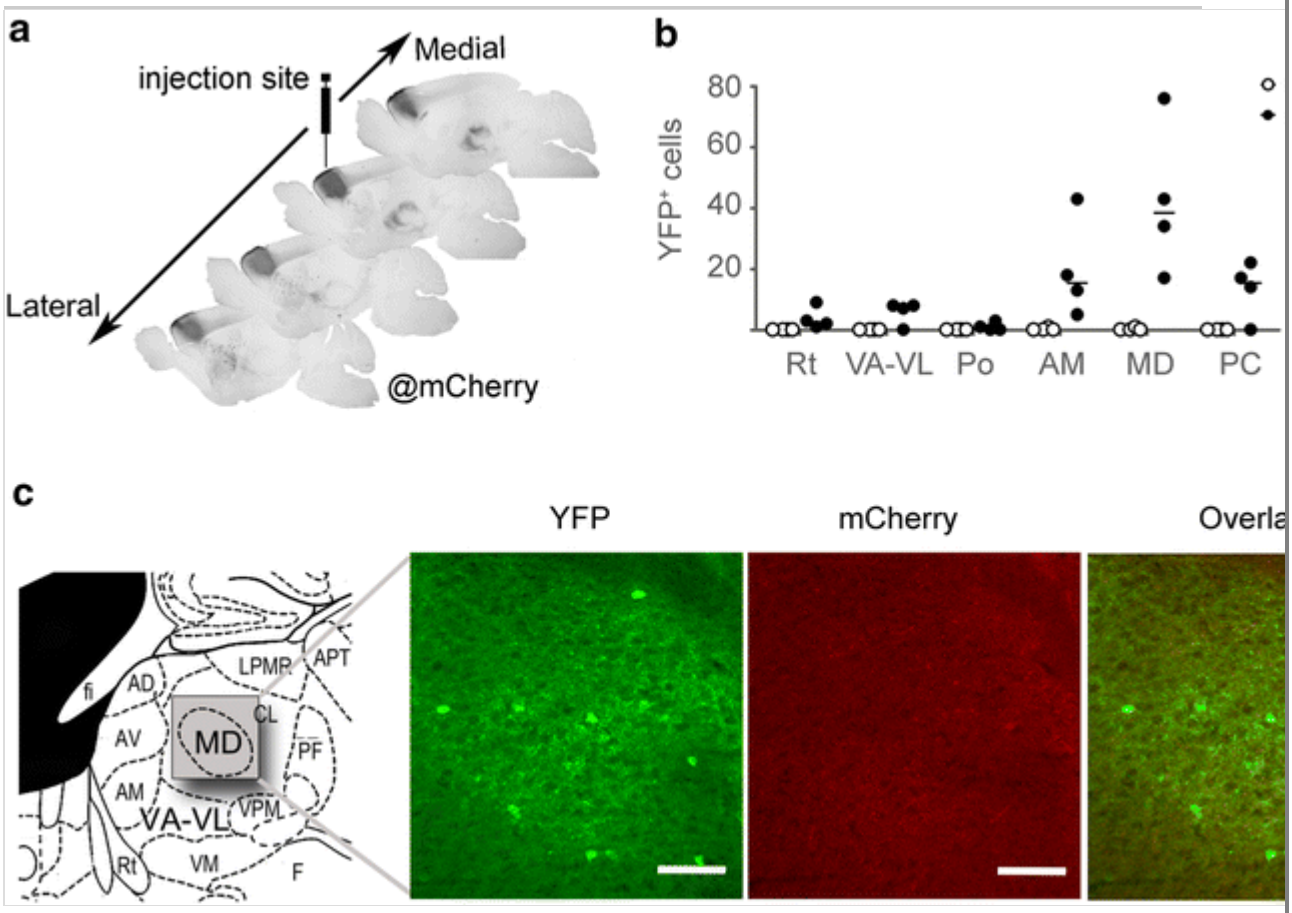

Labeling of the olfactory pathway through sniffing

To assess if the WGA–Cre-dependent transneuronal labeling could visualize the olfactory pathway originating from the nasal epithelium, the viral vector solution was sniffed by spontaneous

respiration into the nasal cavity. Unexpectedly, we could not detect any transneuronal labeling at 6-week p.i. However, immunohistochemical analysis of mCherry expression confirmed a transduction of the nasal epithelium, since mCherry^{+} fiber terminals were present in the OB (Online Resource 10).

WGA–Cre transneuronal labeling shows connectivity to newborn neurons of the OB prior to integration

It has been reported that SVZ-derived newborn neurons arriving in the OB are connected by the surrounding network prior to integration (Deshpande et al. 2013; Kelsch et al. 2009). In an attempt to label the subset of newborn neurons connected by the AON, we injected the rAAV2/7 WGA–Cre in the AON of 8-week-old R26 YFP mice. Immunohistochemical analysis for mCherry 6-week p.i. showed a robust transduction of the AON across the lateromedial axis and mCherry^{+} fiber terminals in the OB (Fig. 7a).

Fig. 7

WGA–Cre tracing shows a connection to newborn neurons in the rostral migratory stream. **a** The anterior olfactory nucleus (AON) encircling the rostral migratory stream (RMS) was targeted by stereotactic injection of the rAAV2/7 WGA–Cre as visible on the mCherry histological staining. The injection site is indicated and sections are 250 μm apart. In the olfactory bulb, ascending mCherry^{+} fibers from the AON are apparent as well as some mCherry^{+} cells. **b** Transneuronally labeled YFP^{+}/mCherry^{-} cells (*filled circles*) and transduced YFP^{+}/mCherry^{+} neurons (*open circles*) were quantified in the granule cell layer (GCL) and the RMS of the OB. The median of $n = 4$ mice is indicated. **c** A representative superimposed tiled confocal *z*-stack of the transduced AON encircling the RMS. Note that the RMS itself is not transduced at the injection site [c first column (1)]. Newborn neurons, apparent from their morphology, are connected and thus YFP^{+}/mCherry^{-} [c middle column (2)]. In the

GCL of the OB, both connected and transduced neurons are visible with a clear mature morphology [c last column (3)]. *AOD* anterior olfactory nucleus; dorsal part, *AOV* anterior olfactory nucleus, ventral part. *Scale bars* 100 μm

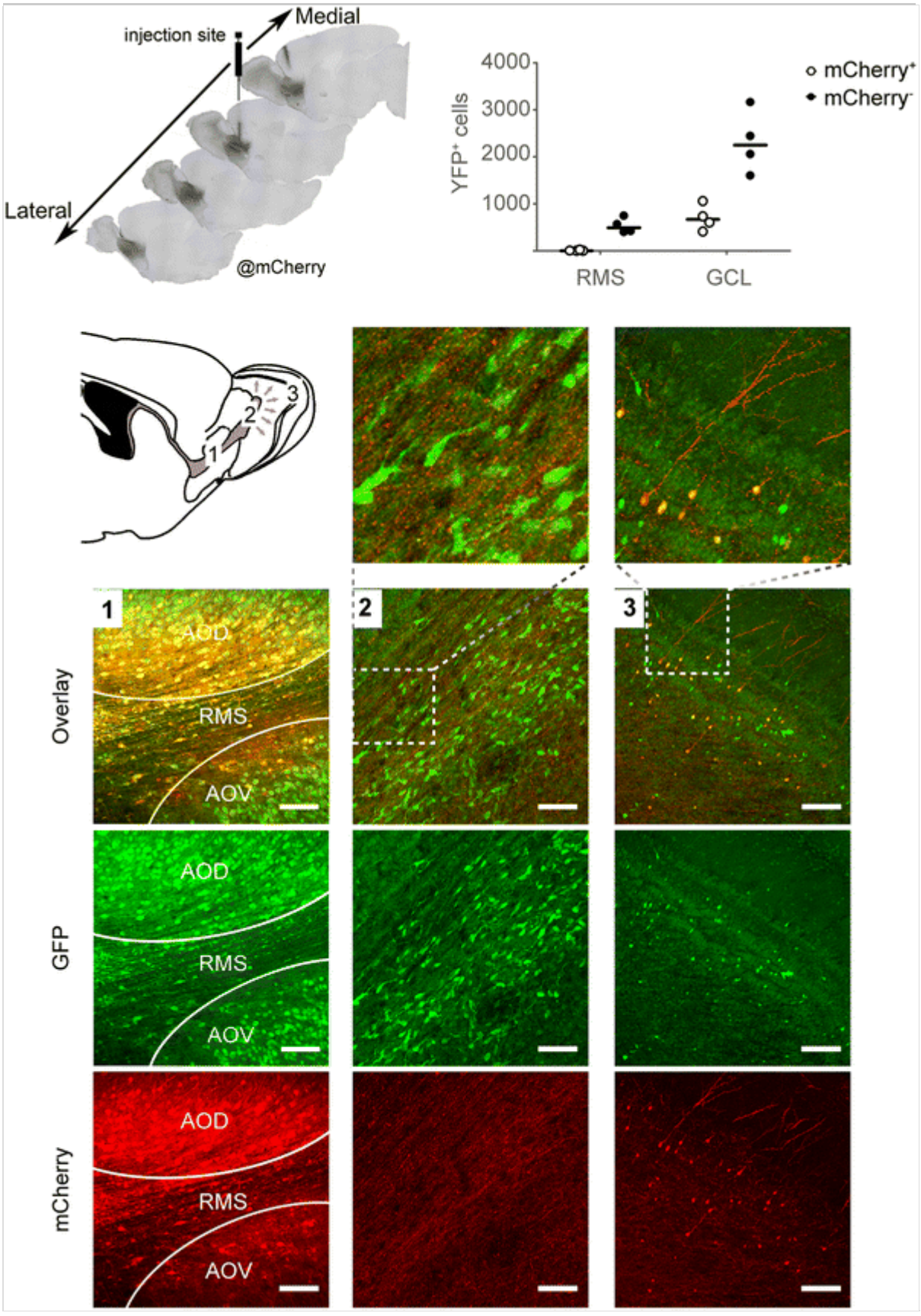

In 4 out of 6 animals, transneuronally labeled $YFP^+/mCherry^-$ cells were visible in the OB, and thus, only in these 4 animals, quantifications were performed (Fig. 7b). Since the AON encircles the RMS where newborn neurons are migrating to the OB, newborn neurons were also transduced upon injection in these animals. At 6-~~week~~weeks p.i., these neurons have migrated to the OB and matured into fully branched transduced granule cells (Fig. 7c bottom panel). Accordingly, almost no residing $YFP^+/mCherry^+$ cells could be found in the RMS at the injection site in the AON (Fig. 7c upper panel). These observations were confirmed on single ~~staining~~stainings against mCherry ~~or~~and YFP with biotinylated antibodies on consecutive sections (Online Resource 11). In the part of the RMS situated in the OB, a high degree of transneuronal labeling with a median of 493 $YFP^+/mCherry^-$ cells (range 400–749) compared with 3 $YFP^+/mCherry^+$ cells (range 0–22) could be quantified (Fig. 7 b, c middle panel). Considering their location and their morphology, these transneuronally labeled neurons just arrived in the OB and did not start their integration process in the bulbar network. In the granule cell layer (GCL), a median of 2250 $YFP^+/mCherry^-$ cells (range 1598–3163) compared with 669 $YFP^+/mCherry^+$ cells (range 408–1059) were found with a mature branched morphology. Hence, both the transduced neurons in the AON and the transduced neurons observed in the GCL may have elicited the transneuronal labeling observed in the bulbar RMS. In the two excluded animals, lacking transneuronally labeled cells in the OB, a similar transduction pattern of the AON was achieved, $mCherry^+$ fiber terminals in the OB were present, but no transduced cells in the GCL occurred. Since no transneuronal labeling seemed to occur when only the AON was transduced, we suggest that the observed transneuronal labeling originated in the transduced mature GCs. Consequently, this implies that matured newborn neurons play an important role in the integration of the subsequent cohort of newborn neurons arriving in the OB.

Discussion

Over the last years, systems neuroscience is more and more focused on deciphering the neuronal networks underlying behavior in normal and diseased phenotypes. To do so, an extensive toolkit to visualize and manipulate these networks on a cellular and circuit level is of high value. However, targeting transgenes to specific subpopulations in the central nervous system based on their neuronal connectivity is not an easy task. Often specific promoters have not yet been characterized rendering the use of the genetic toolbox impossible. A couple of tools have already been developed to visualize synaptically connected neurons ranging from injectable tracer proteins and vector-based expression of tracers to the use of viruses to trace neuronal connections (Lanciego and Wouterlood 2011). All of these have their own advantages and disadvantages, and because of that, it is important to have a range of tools to our disposal for different research questions.

WGA, a plant lectin, has already been known for decades and was first used as an injectable tracer protein and later on expressed in the brain via AAV or adenoviral vectors (Borges and Sidman 1982; Fabian and Coulter 1985; Kinoshita, Mizuno, and Yoshihara 2002; Ruda and Coulter 1982; Yoshihara et al. 1999). Upon expression of WGA in the brain, it is transported bidirectional toward the axons and dendrites where it is presented to the synaptic cleft through exocytosis. Then, it is taken up by the next cell through receptor-mediated endocytosis (Fabian and Coulter 1985). Bidirectional transport of WGA has been documented with preference for anterograde transport, although not all studies are consistent on this. For this reason, we evaluated the transneuronal transport of a fusion protein of WGA and Cre recombinase in ROSA26-loxP-stop-loxP-YFP mice. A rAAV2/7 CMV–mCherry–IRES–WGA–Cre was injected in several mouse brain regions, including the hippocampus, basal ganglia, motor cortex, and AON. In addition, labeling of the olfactory pathway was assessed through sniffing of the viral vector

solution. After 6 weeks, the brains were analyzed via immunohistochemical staining distinguishing transduced cells with an $YFP^{+}/mCherry^{+}$ phenotype and transneuronally labeled cells being $YFP^{+}/mCherry^{-}$.

To determine the kinetics of the labeling, we performed a time course study after WGA–Cre vector transduction in the hippocampus. We observed first a lag phase during which transneuronal labeling stayed rather low. From 3 weeks up to 6 weeks ~~post-injection~~p.i., a steady increase in transneuronally labeled neurons was observed in the targeted areas. This trend was similar in all the connected areas of the hippocampus. However, in the thalamus, the fold increase compared with 1-week ~~post-injection~~p.i. was somewhat lower. Therefore, it appears that the expression levels of WGA need to build up in the transduced cells until they are high enough for transneuronal labeling to occur. These kinetics can in part be explained by the rate-limiting second strand synthesis step of the rAAV-based vector system we employed, which generally peaks at about 2 weeks (Ferrari et al. 1996), together with the time required for the WGA–Cre protein to move about and activate the genomic switch in the connecting cells, which in turn should transcribe and translate the YFP reporter.

We found that for all the transduced regions, except for the nasal epithelium, transneuronal labeling occurred to some extent. However, this labeling was not as efficient in every region. In this study, the highest number of connected cells was quantified for the connection between the hemispheres of the hippocampus. However, we should consider that these quantifications represent absolute values of one-fifth of that region. This number does not consider the volume of the region nor the connectivity strength between two regions. Consequently, it is difficult to compare the labeling in terms of efficiency. Nonetheless, differences in labeling efficacy can be scored based on the occurrence of ‘side effects’ such as off-site transduction that makes it difficult to use the technique to study

neuronal connectivity or to induce specific topological transgene expression. Our results indicate a higher efficacy for elucidating hippocampal circuitry. After injection of the rAAV2/7 WGA–Cre in the hippocampus, connected regions, such as the diagonal band of Broca and MS system, were labeled without the occurrence of transduced ($mCherry^{+}$) cells. Furthermore, also the corticothalamic connection can be detected and studied without the occurrence of transduced cells. In other regions, such as the interhippocampal connectivity and the hippocampal—mammillary nuclei connection, transduced cells do occur. This presence of transduced cells might be explained by retrograde transfer of the viral vector as previously reported (Aschauer et al. 2013; Cearley and Wolfe 2006; Van der Perren et al. 2011; Taymans et al. 2007). Due to interhippocampal reciprocal connectivity, neurons in the cHC could be transduced by viral vector entry in their fiber terminals in the injected side. Also, viral vector spread along the corpus callosum upon injection could also have led to the observed transduction in the cHC.

Nonetheless, it seems that the WGA–Cre-dependent labeling is rather specific. After stereotactic injection of the AAV2/7 Cre control vector, only a small population of seemingly transneuronal Cre-labeled cells occurred. This might be explained by subthreshold mCherry expression or some aspecific transport of the Cre recombinase.

Concerning the directionality of transneuronal labeling, being anterograde or retrograde, different results have been reported. Also, in our study, it was not always easy to deduce the directionality via immunohistochemistry due to the reciprocal properties of several connections, especially for the basal ganglia circuitry and the thalamocortical pathway. Nonetheless, our data indicate that WGA has prevalence for the anterograde direction. This hypothesis is underlined by the lack of transneuronal labeling in some of the strongly retrogradely connected regions. For example, the entorhinal cortex is the strongest projection to the dentate gyrus of the

hippocampus (Witter 2010). In this study, we did not find transneuronal labeling in the entorhinal cortex (data not shown). Nevertheless, we did observe the same assumed retrograde labeling between the two dentate gyri of the hippocampus as reported by Gradinaru et al. (2010), although the retrogradely transduced cells in the contralateral dentate gyrus could also be the source of this labeling. This discrepancy in findings could also be due to the use of a different AAV serotype.

Furthermore, the observed connection between the hippocampus and the thalamus, more specifically the AD, can most probably be explained by anterograde labeling. Indeed, it is established that there is a dense efferent connection from the subiculum of the HC to the AD via the fornix (Saunders and Aggleton 2007). Also, a projection from the AD to the hippocampus via the cingulum was described as well, although, in the rat, the reunions nucleus of the thalamus is the major source of thalamic afferents to the hippocampus (Vertes et al. 2006). Since no labeled cells were observed in the latter nucleus, which would point to retrograde transneuronal labeling, it appears that the labeled YFP^{+}/$mCherry^{-}$ cells observed in the thalamus were a result of anterograde transneuronal tracing from the subiculum of the hippocampus.

Concerning the labeling in the Broca\MS complex, it is well established that this region and the HC are interconnected. On the one hand, it has been reported that the diagonal band of Broca and the MS project to the HC (Meibach and Siegel 1977; Nyakas et al. 1987). On the other hand, a connection from the HC to the diagonal band of Broca\MS complex has been described both through a direct and indirect pathway via the lateral septum. Indeed, pyramidal cells seem to connect to the Broca/MS complex via the lateral septum, while non-pyramidal cells, mostly residing in CA3, seem to connect directly (Gaykema et al. 1991).

Finally, it has been reported that the subiculum of the HC, which is

partially transduced as well, projects via the fornix to the MM suggesting an anterograde WGA–Cre tracing. The SuMM on the other hand is reported as both an afferent and efferent of the HC making it difficult to conclude on the directionality of the labeling observed (Aggleton et al. 2005; Kiss et al. 2002; Sherlock and Raisman 1975; Vann and Aggleton 2004; Zhenzhong et al. 2013).

Considering the efficiency and selectivity of the system, our data indicate that upon expression of the WGA–Cre transgene in a region of interest, not all the connected regions are labeled. For example, we did not observe the known connectivity between the hippocampus and the VTA or hypothalamus (Wyss et al. 1979). Even more striking, the connection from the CA1 and subiculum to the entorhinal cortex (EC), one of the most established connections, was not labeled by the WGA–Cre tracing system (Witter 2010). We did observe some $mCherry^{+}$ terminals arriving in the entorhinal area and some $mCherry^{+}$ cells as well (Online Resource 2). The latter is probably caused by retrograde transport of the viral vector as the EC is also an important input region to the HC. Notably, the mCherry labeling of the terminals was rather weak and local compared with the previous reports (Cenquizca and Swanson 2007). This weaker labeling of transduced terminals in the EC might be due to the fact that the injection site was targeted toward the hilus and the CA3 region, while the terminals toward the EC ascend from the subiculum and CA1. Consequently, the WGA–Cre expression level in the cells connecting to the EC might have been below the critical threshold. Furthermore, in the basal ganglia, we observed a difference in efficacy with a stronger labeling from the SN toward the striatum compared with the labeling from the striatum to the SN. The use of dopamine as a neurotransmitter in the excitatory nigrostriatal connections and GABA in the inhibitory striatonigral connections might play a role in this particular difference in efficacy. In general, the non-uniform distribution of lectin binding sites on the post-synaptic membranes might be a plausible hypothesis for the labeling selectivity (Sawchenko and Gerfen 1985; Schnyder and

Künzle 1983). It has also been hypothesized that stronger connections will be labeled faster than weaker connections (Schnyder and Künzle 1983). However, in our study, this cannot explain the observed difference in basal ganglia labeling, since the less efficiently labeled nigrostriatal connection is known to be a dense innervation (Gerfen 2004). Furthermore, the degree of axonal transport taking place in that population of neurons has been stated to have an influence (Schnyder and Künzle 1983). Finally, it is possible that some synaptic geometries are not conducive to transfer (Sawchenko and Gerfen 1985). Also, not only the binding sites for WGA could lead to labeling selectivity, but also the viral vector entry depends on the presence of certain receptors. It has been reported that different serotypes of AAV enter the cell via specific cell surface glycan receptors (Braz et al. 2002; Kinoshita et al. 2002; Ruda and Coulter 1982; Schnyder and Künzle 1983). The differences in glycan architecture throughout the brain could contribute to variation in the efficiency of gene transfer by AAV capsids and, thus, lead to a selectivity of transduction of first-order neurons. Consequently, some connections of which the first-order neurons do not or not sufficiently express the specific glycan receptor might remain undetected.

Although different studies have reported that WGA has the capability of visualizing multisynaptic pathways, we found no clear evidence for this in our study. In the case of the hippocampal circuits, there are strong innervations of the HC toward the lateral septum which in their turn project to the medial septum (MS) and diagonal band of Broca complex. Consequently, the transneuronal labeling observed in the latter could be a result of disynaptic labeling. However, throughout the animal group, we found no correlation between the amount of transneuronal labeling in the MS/Broca complex and the lateral septum. Furthermore, in one animal, no labeling in the lateral septum was found, while transneuronal labeling in the MS/Broca complex was evident. We, therefore, conclude that we mostly observe monosynaptic

transneuronal labeling in this system and in this time window. Furthermore, if there would be a significant labeling of the second-order nuclei, more labeling should have occurred in relay nuclei, such as the thalamus and hypothalamus.

Remarkably and somewhat against our expectations, no transneuronal labeling in the olfactory bulb was observed after nasal administration of the viral vector solution, despite of efficient transduction of the fiber terminals arriving in the OB (Online Resource 10). Yoshihara et al. reported that WGA transfer across synapses seemed to depend on the expression levels of the WGA protein in the first-order neurons. They used a strong OMP promoter to drive the expression in the nasal epithelium (Yoshihara et al. 1999). They also showed that with adenoviral expression of WGA driven by the ubiquitous promoter CAG, transneuronal labeling was still observed, although already weaker (Zhao et al. 1996). The AAV2/7 viral vector used in our study might not be the most suitable serotype for nasal transduction. This in combination with ~~a~~an ubiquitous promoter might lead to lower expression levels and thus explain the lack of transneuronal labeling. Also, previous studies mostly expressed a single WGA transgene, while the fusion of Cre recombinase and WGA might affect protein activity in a mild manner and, consequently, lead to less efficient transneuronal labeling (Kinoshita et al. 2002; Yoshihara 2002; Yoshihara et al. 1999). On the other hand, using a WGA–Cre fusion protein has the advantage of inducing stable gene expression in inducible transgenic mice. This solves the problem of transient transneuronal labeling as observed as well for the olfactory pathway (Kinoshita et al. 2002).

Besides labeling of connections in the mature nervous system, we wanted to label newborn neurons in the SVZ-OB pathway to visualize their connectivity to the AON prior to integration in the adult neuronal network in the OB. However, we did not observe any transneuronal labeling after transduction of the AON. Yet, it has been reported using RV-mediated retrograde tracing that the AON

makes contact with the SVZ derived newborn neurons prior to their integration in the bulbar network (Deshpande et al. 2013). Nevertheless, in some animals, we did observe labeled newborn neurons during their migration in the bulbar part of the RMS, but this labeling was not due to transduction of AON neurons. During stereotactic injection, not only the AON but also some migrating neurons in the RMS ensheathed by the AON were transduced. Upon analysis 6-week p.i., these cells had already matured and appeared as transduced granule cells. Because we only observed transneuronal labeling when these cells were transduced, we conclude that these cells are responsible for the transneuronal labeling in the bulbar RMS. Of note, the newborn neurons in the bulbar RMS, which were transneuronally labeled, seemed to be of an earlier time point as described by Deshpande et al. In their study, they focused on time points starting from the moment where the progenitors leave the RMS and continue their radial migration and differentiation in the bulbar layers.

A drawback of the WGA–Cre-dependent circuit tracing is the observed direct transduction of neurons in distal areas, including the connected regions. It has been reported that some AAV serotypes appear to transduce distal neurons upon cell entry via the fiber terminals in the injection site. Consequent retrograde transfer to the cell body could then result in transduced neurons several mm away (Castle et al. 2014). Since this characteristic seems to depend upon the serotype and the region of interest, retrograde transfer could be limited by the use of the right serotype for the application (Aschauer et al. 2013; Cearley and Wolfe 2006; Van der Perren et al. 2011; Taymans et al. 2007). We used a serotype which in our experience has a very broad tropism to compare the labeling efficacy in different brain regions (Taymans et al. 2007). Furthermore, anterograde transfer of the viral vector upon cell entry and subsequent secretion at the synapse has been reported to result in transduction of connected neurons, however, resulting in lower expression levels (Castle et al. 2014). The latter could also explain

the observed YFP^{+}/$mCherry^{-}$ cells after injection with the Cre control vector. Anterograde transfer of AAV requires a higher level of AAV uptake than for transduction of the first order neuron, and as such, this side effect could be lowered by optimization of the viral vector dose (Castle et al. 2014). To target precise neuronal subpopulations, specific promoters in combination with transgenic animals can be used instead of the ubiquitous CMV promoter used in this study.

Unlike neurotropic viruses, WGA circuit tracing could leave weaker connections undetected. Furthermore, the efficiency of transneuronal transport of neurotropic viruses, such as the herpes viruses and the rabies virus, is much higher. Neurotropic viruses spread through the nervous system as part of their natural life cycle, and hence, the transgene is amplified after the transneuronal spread. WGA is efficiently taken up by neurons due to the binding affinity to glycolipids on the membrane. However, once inside the cell, the transport largely depends on the vesicle transport of the cell rendering this labeling system less efficient compared with neurotropic viruses. On the other hand, cytotoxicity is a major concern when using neurotropic viruses. As a consequence, these viruses are less suited for long-term experiments unlike WGA–Cre-dependent labeling (Callaway 2008; Kelly and Strick 2003; Viral et al. 2012). Besides, Gradinaru et al. showed that WGA–Cre-dependent labeling provides ample topologic expression for circuit manipulation by channelrhodopsins (Gradinaru et al. 2010). Finally, the transsynaptic aspect of the WGA–Cre tracer system is a major advantage compared with the canine adenovirus type 2 (CAV2) viral vectors. The high disposition for retrograde axonal transport in vivo makes the CAV2 vector, a useful tool in the labeling of projecting neurons (Junyent and Kremer 2015). However, upon transduction of axon termini, only the distant population of connecting neurons is labeled, whereas with the WGA–Cre system, both the pre-synaptic and the post-synaptic neurons can be visualized.

In conclusion, we have shown that the WGA–Cre-dependent topological transgene expression can be a useful tool to manipulate and modulate neuronal connectivity. In combination with transgenic animals or Cre-dependent viral vectors encoding transgenes, such as light-activated channels or DREADDs, new possibilities arise to couple specific neuronal networks to their physiological outputs. Especially, the possibility of long-term modulation overcomes the major shortcoming of tracing viruses, such as RV; however, the labeling efficiency is lower. With this study, we provide a detailed analysis of the applicability of the system in mouse brain. We can conclude that the transneuronal tracer capacity of the WGA lectin is different for specific neuronal connections and dependent on the time window. Additional techniques, such as electrophysiology, might further clarify the directionality of the labeling.

Acknowledgments

The authors would like to thank the Leuven Viral Vector Core for the construction and production of the rAAV vectors and Prof Lieve Moons and Prof Lut Arckens for the use of the confocal laser scanning microscope. The research presented in this paper has received funding from the Fund for Scientific Research-Flanders (FWO—fellowship to SL), the European projects FP7-ICT-2011-C-284801 ENLIGHTENMENT and FP7 HEALTH-F2-2011-278850 (INMiND), the Flemish Agency for Innovation through Science and Technology (IWT—SBO/110068 Optobrain) and the KU Leuven (OT/14/120).

Electronic supplementary material

Below is the link to the electronic supplementary material.

Supplementary material 1 (PDF 2151 kb)

References

Aggleton JP, Vann SD, Saunders RC (2005) Projections from the Hippocampal Region to the mammillary bodies in macaque monkeys. Eur J Neurosci 22:2519–2530

Andersen P, Morris R, Amaral D, Bliss T, O'Keefe J (2006) The hippocampus book. Oxford University Press, Oxford

Aschauer DF, Kreuz S, Rumpel S (2013) Analysis of transduction efficiency, tropism and axonal transport of AAV serotypes 1, 2, 5, 6, 8 and 9 in the mouse brain. PLoS One 8(9):1–16

Aston-Jones G, Card JP (2000) Use of pseudorabies virus to delineate multisynaptic circuits in brain: opportunities and limitations. J Neurosci Methods 103(1):51–61

Boldogköi Z, Sík A, Dénes Á, Reichart A, Toldi J, Gerendai I, Kovács KJ, Palkovits M (2004) Novel tracing paradigms —genetically engineered herpesviruses as tools for mapping functional circuits within the CNS: present status and future prospects. Prog Neurobiol 72(6):417–445

Borges LF, Sidman RL (1982) Axonal transport of lectins in the peripheral nervous system. J Neurosci 2(5):647–653

Braz JM, Rico B, Basbaum AI (2002) Transneuronal tracing of diverse CNS circuits by cre-mediated induction of wheat germ agglutinin in transgenic mice. Proc Natl Acad Sci USA 99(23):15148–15153

Callaway Edward M (2008) Transneuronal circuit tracing with neurotropic viruses. Curr Opin Neurobiol 18(6):617–623

Carretta D, Sbriccoli A, Santarelli M, Pinto F, Granato A, Minciacchi D (1996) Crossed thalamo-cortical and cortico-thalamic projections in adult mice. Neurosci Lett

204(1–2):69–72

Castle MJ, Gershenson ZT, Giles AR, Holzbaur ELF, Wolfe JH (2014) Adeno-associated virus serotypes 1, 8, and 9 share conserved mechanisms for anterograde and retrograde axonal transport. Hum Gene Ther 25(8):705–720

Cearley CN, Wolfe JH (2006) Transduction characteristics of adeno-associated virus vectors expressing cap serotypes 7, 8, 9, and Rh10 in the mouse brain. Mol Ther 13(3):528–537

Cenquizca LA, Swanson LW (2007) Spatial organization of direct hippocampal field CA1 axonal projections to the rest of the cerebral cortex. Brain Res Rev 56(1): 1–26. http://www.pubmedcentral.nih.gov /articlerender.fcgi?artid=2171036&tool=pmcentrez& rendertype=abstract. Accessed Nov 11, 2012)

Deniau JM (1994) Indirect nucleus accumbens input to the prefrontal cortex via the substantia nigra pars reticulata: a combined anatomical and electrophysiological study in the rat. Neuroscience 61(3):533–545

Deshpande A, Bergami M, Ghanem A, Conzelmann K, Lepier A, Götz M, Berninger B (2013) Retrograde monosynaptic tracing reveals the temporal evolution of inputs onto new neurons in the adult dentate gyrus and olfactory bulb. Proc Natl Acad Sci USA 110(12):1152–1161

Fabian RH, Coulter JD (1985) Transneuronal transport of lectins. Brain Res 344(1):41–48

Ferrari FK, Samulski T, Shenk T, Samulski RJ (1996) Second-strand synthesis is a rate-limiting step for efficient transduction by recombinant adeno-associated virus vectors. J Virol

70(5):3227–3234

Gaykema RPA, Van Der Kuil J, Hersh LB, Luiten PGM (1991) Patterns of direct projections from the hippocampus to the medial septum-diagonal band complex: anterograde tracing with phaseolus vulgaris leucoagglutinin combined with immunohistochemistry of choline acetyltransferase. Neuroscience 43(2/3):349–360

Gerfen CR (2004) Basal Ganglia. In: Paxinos G (ed) The rat nervous system. Elsevier academic press, Amsterdam, p 455–508

Ginger M, Haberl M, Conzelmann K, Schwarz MK, Frick A (2013) Revealing the secrets of neuronal circuits with recombinant rabies virus technology. Front Neural Circuits 7(January):2

Gradinaru V, Zhang F, Ramakrishnan C, Mattis J, Prakash R, Diester I, Goshen I, Thompson KR, Deisseroth K (2010) Molecular and cellular approaches for diversifying and extending optogenetics. Cell 141(1):154–165

Haber S, McFarland NR (2001) The place of the thalamus in frontal cortical-basal ganglia circuits. The Neuroscientist 7(4):315–324

Joel D, Weiner I (2000) Commentary. the connections of the dopaminergic system with the striatum in rats and primates: an analysis with respect to the functional and compartmental organization of the striatum. Neuroscience 96(3):451–474

Junyent Felix, Kremer Eric J (2015) CAV-2-why a canine virus is a neurobiologist’s best friend. Curr Opin Pharmacol 24:86–93

Kelly RM, Strick PL (2003) Rabies as a transneuronal tarcer of

circuits in the central nervous system. J Neurosci Meths 103:63–71

Kelsch W, Lin C, Mosley CP, Lois C (2009) A critical period for activity-dependent synaptic development during olfactory bulb adult neurogenesis. J Neurosci 29(38):11852–11858

Kinoshita N, Mizuno T, Yoshihara Y (2002) Adenovirus-mediated WGA gene delivery for transsynaptic labeling of mouse olfactory pathways. Chem Senses 27(3):215–223

Kiss J, Csaki H, Bokor H, Kocsis K, Kocsis B (2002) Possible glutamatergic/aspartatergic projections to the supramammillary nucleus and their origins in the rat studied by selective [3H] D-aspartate labelling and immunocytochemistry. Neuroscience 111(3):671–691

Lanciego JL, Wouterlood FG (2011) A half century of experimental neuroanatomical tracing. J Chem Neuroanat 42(3):157–183

Meibach CR, Siegel A (1977) Efferent connections of the septal area in the rat : an analysis utilizing retrograde and anterograde transport methods. Brain Res 119:1–20

Ming G, Song H (2011) Adult neurogenesis in the mammalian brain: significant answers and significant questions. Neuron 70(4):687–702

Nyakas C, Luiten PGM, Spencer DG, Traber J (1987) Detailed projection patterns of septal and diagonal band efferents to the hippocampus in the rat with emphasis on innervation of CA1 and dentate Gyrus. Brain Res Bull 18(4):533–545

Paxinos G, Franklin KBJ (2004) The mouse brain in stereotaxic

coordinates
AQ2

Rouiller EM, Welker E (2000) A comparative analysis of the morphology of corticothalamic projections in mammals. Brain Res Bull 53(6):727–741

Ruda M, Coulter JD (1982) Axonal and transneuronal transport of wheat germ agglutinin demonstrated by immunocytochemistry. Brain Res 249:237–246

Saunders RC, Aggleton JP (2007) Origin and topography of fibers contributing to the fornix in macaque monkeys. Hippocampus 17:396–411

Sawchenko PE, Gerfen CR (1985) Plant lectins and bacterial toxins as tools for tracing neuronal connections. Trends Neurosci 8:378–384

Schnyder H, Künzle H (1983) Differential labeling in neuronal tracing with wheat germ agglutinin. Neurosci Lett 35(2): 115–20. http://linkinghub.elsevier.com/retrieve/pii/0304394083905372
AQ3

Sherlock DA, Raisman G (1975) A comparison of anterograde and retrograde axonal transport of horseradish peroxidase in the connections of the mammillary nuclei in the rat. Brain Res 85:321–324

Srinivas S, Watanabe T, Lin CS, William CM, Tanabe Y, Jessell TM, Costantini F (2001) Cre reporter strains produced by targeted insertion of EYFP and ECFP into the ROSA26 locus. BMC Dev Biol 1:4

Taymans J, Vandenberghe LH, Van Den Haute C, Thiry I,

Deroose CM, Mortelmans L, Wilson JM, Debyser Z, Baekelandt V (2007) Comparative analysis of adeno-associated viral vector serotypes 1, 2, 5, 7, and 8 in mouse brain. Hum Gene Ther 18(3):195–206

Van der Perren A, Toelen J, Carlon M, Van den Haute C, Coun F, Heeman B, Reumers V, Vandenberghe LH, Wilson JM, Debyser Z, Baekelandt V (2011) Efficient and stable transduction of dopaminergic neurons in rat substantia nigra by rAAV 2/1, 2/2, 2/5, 2/6.2, 2/7, 2/8 and 2/9. Gene Ther 18(5):517–527

Vann SD, Aggleton JP (2004) The mammillary bodies: two memory systems in one? Nature reviews. Neuroscience 5:35–44
AQ4

Vertes RP, Hoover WB, Do Valle AC, Sherman A, Rodriguez JJ (2006) Efferent projections of reuniens and rhomboid nuclei of the thalamus in the rat. J Comp Neurol 499:768–796

Viral (2012) Anterograde trans-synaptic, tracer for, mapping output, pathways of, and genetically marked neurons. NIH Public Access 72(6): 938–50

Voorn P, Vanderschuren LJ, Groenewegen HJ, Robbins TW, Pennartz CM (2004) Putting a spin on the dorsal-ventral divide of the striatum. Trends Neurosci 27(8):468–474

Whitman MC, Greer CA (2007) Synaptic integration of adult-generated olfactory bulb granule cells: basal axodendritic centrifugal input precedes apical dendrodendritic local circuits. J Neurosci 27(37):9951–9961

Witter MP (2010) Connectivity of the Hippocampus (eds) Vassilis Cutsuridis, Bruce Graham, Stuart Cobb, and Imre Vida. Hippocampal Microcircuits: 5–26

Witter PM, Amaral GD (2004) Hippocampal formation. In: Paxinos George (ed) The Rat central nervous system. Elsevier Academic press, San Diego, pp 705–727

Wyss JM, Swanson LW, Cowan WM (1979) A study of subcortical afferent to the hippocampal formation in the rat. Neuroscience 4:463–476

Yoshihara Y (2002) Visualizing selective neural pathways with WGA transgene: combination of neuroanatomy with gene technology. Neurosci Res 44(2):133–140

Yoshihara Y, Mizuno T, Nakahira M, Kawasaki M, Watanabe Y, Kagamiyama H, Jishage K, Ueda O, Suzuki H, Tabuchi K, Sawamoto K, Okano H, Noda T, Mori K (1999) A genetic approach to visualization of multisynaptic neural pathways using plant lectin transgene. Neuron 22(1):33–41

Zhao H, Otaki JM, Firestein S (1996) Adenovirus-mediated gene transfer in olfactory neurons in vivo. J Neurobiol 30(4):521–530

Zhenzhong C, Gerfen CR, Young WS (2013) Hypothalamic and other connections with the dorsal CA2 area of the mouse hippocampus. J Comp Neurol 521(8):1844–1866